
# High-flux source of coherent XUV pulses for user applications

Research Article | Vol. 27, No. 6 | 18 Mar 2019 | OPTICS EXPRESS 8871
Optics EXPRESS

# High-flux source of coherent XUV pulses for user applications

O. Hort,[1,*] M. Albrecht,[1,2] V. E. Nefedova[1,2] O. Finke,[1,2] D. D. Mai,[1] S. Reyné,[3] F. Giambruno,[3] F. Frassetto,[4] L. Poletto,[4] J. Andreasson,[1,5] J. Gautier,[1,6] S. Sebban,[1,6] and J. Nejdl[1]

[1]*Institute of Physics of the ASCR, ELI-Beamlines project, Na Slovance 2, 182 21 Prague, Czech Republic*
[2]*Faculty of Nuclear Sciences and Physical Engineering CTU, Brehova 7, 115 19 Prague 1, Czech Republic*
[3]*ARDOP Industrie, Cité de la Photonique, 11 Avenue de Canteranne 33600 Pessac, France*
[4]*Institute of Photonics and Nanotechnologies, National Council for Research, Via Trasea 7, 35131, Padova, Italy*
[5]*Condensed Matter Physics, Department of Physics, Chalmers University of Technology, Gothenburg, Sweden*
[6]*Laboratoire d'Optique Appliquée, 181 Chemin de la Huniére et des Joncherettes, Palaiseau Ile-de-France, France*
[*]*Ondrej.Hort@eli-beams.eu*

**Abstract:** We present experimental results obtained at a user-oriented XUV beamline implemented at the ELI Beamlines facility. The coherent XUV radiation is produced via high harmonic generation in gases in a loose focusing geometry. The beamline is designed to be driven by 1 kHz, 100 mJ, 20 fs pulses centered at a wavelength of 830 nm. Results such as XUV spectra, beam wavefront and pulse energy obtained during the beamline commissioning with a commercial 1 kHz, 5 mJ, 40 fs laser system are presented. A unique XUV spectrometer for source characterization designed to reach a very high sensitivity is described in detail, and we demonstrate a novel technique for single-shot and every-shot XUV pulse energy measurement.



## 1. Introduction

The coherent extreme ultra-violet (XUV) pulses, produced via high-order harmonic generation (HHG) in gases, are now the main workhorse for scientific applications such as probing the dynamics of atomic and molecular electronic structures on attosecond timescales [1, 2] and are also finding uses in coherent diffractive imaging of both fixed targets [3, 4] and isolated He clusters [5].

For applications requiring mainly XUV photon energies, ultrashort pulses (even sub-fs) and highly synchronized pump and probe pulses, HHG sources are unrivaled. However, for photon hungry applications, such as single shot coherent diffractive imaging, the applicability of HHG sources is limited by the low XUV photon flux due to low conversion efficiency of the HHG process. A number of approaches to increase the photon flux are being investigated, including quasi-phase matching [6] or HHG driven by two-color laser field [7].

Another approach to increase the XUV pulse energy which consists of using high energy femtosecond pulses in a long focusing geometry to increase the generating medium volume while keeping the ionization at the optimal level [8, 9]. Recent advances in laser technology indicates this as an interesting way forward.

Recently, a lot of effort has been devoted to combining the advantages of optical parametric amplification (OPA) and Ti:Sapphire based lasers. This new generation of laser systems should be able to deliver very short pulses with pulse duration of < 20 fs at a repetition rate of 1 kHz and a pulse energy exceeding 100 mJ. Such kind of laser system is being developed at the ELI Beamlines facility [10] where it will be used to drive a user-oriented XUV beamline based on

#351945 https://doi.org/10.1364/OE.27.008871
Journal © 2019 Received 15 Nov 2018; revised 25 Dec 2018; accepted 31 Dec 2018; published 12 Mar 2019

Optics EXPRESS

HHG in gas targets. In this article we present the following: HHG beamline of the ELI Beamlines facility; experimental results obtained during instrument commissioning using a 5 mJ, 40 fs, 1 kHz Ti:Sapphire laser system; expected parameters of the XUV pulses generated with the new generation of near IR kHz laser driver; all XUV and laser diagnostics included in the beamline; and upgrades of the system to be implemented in the near future.

The paper is divided into three major sections. First we briefly introduce HHG in gases giving more details about the generation geometries and corresponding outputs. Driving beam alignment and rejection after the generation are discussed as well. The second section contains a description of diagnostic devices and techniques used for the XUV characterization. A unique design of high-sensitivity XUV spectrometer and a novel technique of online XUV pulse energy monitoring are explained in more details. In the last section a monochromator upgrade is described as it will be installed in the beamline in the near future.

## 2. Generation of the XUV beam

### 2.1. HHG scaling

The process of the HHG can be explained using the so called three-step model [11]. It is a semi-classical description of a single-atom response to the high electric field of the intense driving pulse. When the intensity of the laser pulse is high enough it allows an electron to tunnel out through an altered potential barrier. Afterwards the liberated electron is further accelerated by the driving field; then stopped and accelerated backwards. In the vicinity of the parent ion the electron may recombine and emit an XUV photon whose energy equals the sum of the ionization potential of the atom and the kinetic energy acquired under the influence of the driving field.

In addition to the microscopic single-atom response, macroscopic effects influence the output XUV radiation significantly. Phase-matching [12], as an example of macroscopic effects, can rise or inhibit the XUV yield according to constructive or destructive interference of the XUV field in the medium depending on medium length, gas pressure profile and driving pulse characteristics.

For each atomic species, there is an optimal driving laser intensity for harmonic generation, which needs to be high enough to provide both ionization of atoms and the required kinetic energy of electrons returning to the parent ions. The applied intensity should, however, not over-ionize the medium. If this happens, the harmonic signal build-up would be inhibited due to phase-mismatch introduced by the high free electron density and the microscopic process is disabled due to depletion of the atomic ground state.

The previous studies [8, 9] demonstrated that under optimum phase-matching conditions the conversion efficiency for a specific driving laser wavelength and pulse duration does not depend on f-number ($F_\#$) of the driving beam. To give an example, the various focusing conditions (defined by $F_\#$) are featured by different optimal parameters for HHG. The pressure scales as $\frac{1}{F_\#^2}$, while the gas cell length scales as $F_\#^2$. Furthemore, the produced XUV beam demonstrates the decrease of divergence with increasing $F_\#$ [9, 13].

The HHG beamline described in this paper was designed for the laser system L1 [14] generating 20 fs pulses with central wavelength 830 nm and energy of 100 mJ at repetition rate of 1 kHz. This laser system is currently under development at ELI Beamlines. The beamline with all its diagnostics was verified with a commercial laser system delivering pulses of 5 mJ of energy at 1 kHz repetition rate, with central wavelength of about 800 nm, 40 fs pulse duration, beam diameter of 36 mm (at $1/e^2$) and $M^2 < 1.25$.

Table 1 shows the parameters of the XUV pulses generated in different noble gases that were measured during the verification of the HHG beamline with the commercial laser and the parameters expected at optimal conditions with a driver of L1 design parameters. The Rayleigh range $z_R = \frac{4\lambda_0}{\pi} F_\#^2$ ($\lambda_0$ denotes the laser central wavelength), which is comparable to an optimal medium length, using the commercial 5 mJ laser system was 6.4 cm, 1.22 cm, 0.55 cm given by

Optics EXPRESS

Table 1. Expected input and output parameters of the user-oriented high-order harmonic source with 1 kHz repetition rate lasers. Notation: divergence is considered as an angle between the optical axis and direction where the intensity drops to $\frac{1}{e^2}$. The output parameters of XUV pulses generated in helium are estimated based on scaling in the case of both laser drivers.

| Laser system | Gas | XUV wavelength (nm) | Driver $F_{\#}$ | XUV pulse energy (μJ) | XUV divergence (mrad) |
|---|---|---|---|---|---|
| 5 mJ, 40 fs | Xenon | ≥ 51 | 280 | 0.05 | 0.6 |
| 100 mJ, 20 fs | | | 1430 | 2 | 0.1 |
| 5 mJ, 40 fs | Argon | ≥ 32 | 120 | 0.005 | 0.8 |
| 100 mJ, 20 fs | | | 625 | 0.2 | 0.15 |
| 5 mJ, 40 fs | Neon | ≥ 13.5 | 87 | $5\times10^{-4}$ | 0.48 |
| 100 mJ, 20 fs | | | 444 | 0.02 | 0.09 |
| 5 mJ, 40 fs | Helium | ≥ 10 | 75 | $5\times10^{-4}$ | 0.4 |
| 100 mJ, 20 fs | | | 380 | 0.02 | 0.07 |

focal length of 5 m, 3 m, and 2 m for HHG in xenon, argon, and neon, respectively.

Much longer optimal medium lengths are expected with design parameters of the L1 driving laser system. The conversion efficiency (ratio of energy of output harmonic pulse to driving laser pulse energy) is typically of the order of $10^{-5}$, $10^{-6}$ and $10^{-8}$ for Xe, Ar and Ne gases, respectively [15, 16].

### 2.2. *Driving laser focusing geometries and operation modes*

The user-oriented HHG beamline at ELI-Beamlines is a unique system, whose main advantage is the delivery of an intense harmonic beam in various wavelength ranges for photon demanding applications. The HHG beamline is designed in a way of convenient focal length adaptation depending on experimental goals. Spherical mirrors providing focal lengths of 2.5, 5, 8, 12.5, 20, and 25 m resulting in f-numbers 90, 180, 290, 450, 730, and 900, respectively, will be used for focusing of the driving beam.

The HHG beamline consists of 4 large vacuum chambers (VCs) and one small chamber referred to as the filter box (FB), connected with DN250 and DN40 tubes, respectively. The vacuum chambers are positioned in-line in the order VC1 – VC2 – VC3 – FB – VC4. The 3D model of the system is shown in Fig. 1.

The IR driving beam enters the interaction chamber VC2. The vacuum chambers VC3 and VC1 are used to focus and fold the beam depending on the selected focal length. The distance between the chambers VC1, which is the only movable chamber, and the harmonic generation chamber VC2 can be adjusted. Various ensembles of tubes allow the implementation of different focal lengths in a convenient manner. The gas cell for HHG is located in VC2 and the variation of driving beam focus position relative to the gas cell is allowed by a 0.5 m long motorized stage in VC1. The position of the gas cell is fixed for all configurations to ensure the same position of the source, and thus proper imaging needed for diagnostics.

Additionally, the HHG source is designed in a way that allows the generation of high-order harmonics from a two-color driving field. The detailed arrangement for this scenario in VC2

Optics EXPRESS

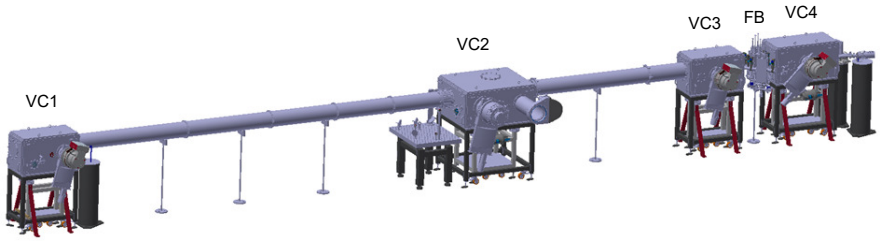


Fig. 1. The 3D model of the HHG beamline at ELI-Beamlines facility.

is shown in Fig. 2. In the simplest case the red beam represents the driving beam with central wavelength of 830 nm and the blue is its second harmonic beam.

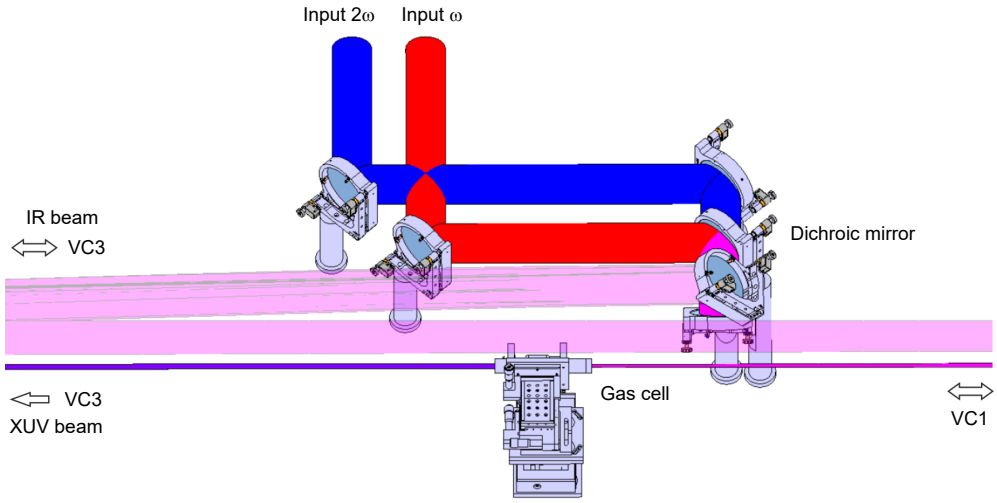


Fig. 2. Schematics of VC2 for two-color HHG. Here, the long focusing geometry is depicted, where the two-color beams are combined via a dichroic mirror and elevated by a periscope to be reflected on the focusing mirror located in VC3. VC1 then contains 2 mirrors to steer the beam to the lower optical axis – the axis of the gas cell and XUV diagnostics.

Furthermore, our unique design supports the possibility of implementing a second gas cell. In this configuration, two high harmonic beams will be generated in separate gas cells by independent parallel driving beams. This way, one can freely define different geometry, driving intensity and gas target for each XUV beam and use them for advanced pump-probe experiments in XUV/soft X-rays.

There are two output arms of the beamline as depicted in Fig. 3. The straight arm is going through the diagnostics chamber (VC4) into the Multipurpose Atomic molecular and optical science and Coherent diffraction imaging chamber (MAC), whose design is similar to the CAMP chamber initially implemented at the AMO station of the LCLS Free Electron Laser and currently in use at FLASH [17]. By inserting a SiC mirror with grazing angle of 20 deg the output beam can be sent to the side arm with a VUV magneto-optical ellipsometer for material science and surface experiments [18].

Optics EXPRESS

### 2.3. Laser alignment system

The driving infrared beam incoming to the HHG beamline enters first the VC2 and has to be aligned onto the beamline axis. There are two independent alignment systems to achieve the fine alignment needed for the HHG. Both systems rely on a two-references/two-mirrors procedure where the first motorized mirror sets the beam to the first reference called near-field, the second mirror to the second reference (far-field). This procedure can be iteratively repeated until the beam is properly set to both references that define the axis. We use CCD and CMOS cameras as the references.

The first alignment system is placed at the laser beam entrance of the HHG beamline and ensures correct injection of the beam into the beamline. The second system is dedicated for fine alignment of the laser beam into the gas cell where the HHG occurs. This beam defines the optical axis of the generated XUV beam.

### 2.4. Laser light rejection system

There are two systems available to remove the laser light from the generated beam and leave only the XUV radiation entering the diagnostics chamber and/or end stations located at the beamline: 1. a set of 3 grazing incidence fused silica flat mirrors that reduce the driving laser flux by about two orders of magnitude and 2. two independent sets of thin metallic filters that filter out the residual laser light.

The vacuum chamber VC3 contains 3 IR AR-coated mirrors under grazing angles 3, 6, and 3 degrees that preserve the original beam axis (see Fig. 3). The majority of the IR light is transmitted by these mirrors and dumped, while the XUV beam is reflected thanks to the low grazing angle. The last layer of the coating is composed of SiC in order to increase the reflectivity for the lower energy part of the spectral range (with estimated throughput above 0.7 for radiation wavelength above 20 nm / below 60 eV of photon energy) corresponding to efficient HHG in heavy noble gases. As discussed above, HHG in those gases will be performed with large f-numbers resulting in higher driving power in small beam.

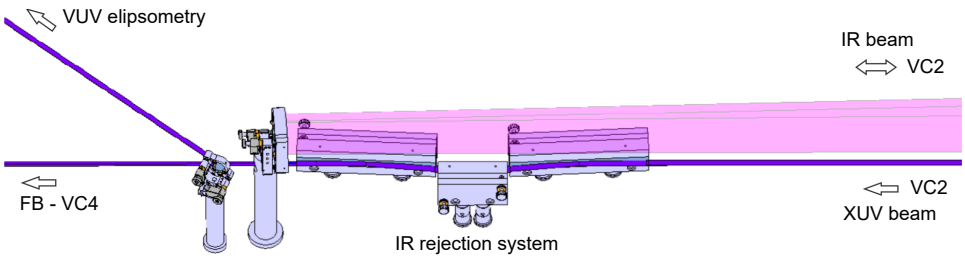


Fig. 3. Schematic of VC3. From left to right: removable mirror designed to steer the XUV beam to ellipsometry setup, folding or focusing mirror (depending on the focal length), IR rejection system.

Following the 3-mirror set there are two sets of thin metallic filters located in the filter box chamber to block the residual laser light. In each set, 5 different filters can be exchanged directly under vacuum. Aluminum, zirconium and indium are the standard set of filters to cover the required wavelength range. The FB chamber can be vented and pumped separately to allow quick exchange of the metallic filters.

## 3. Diagnostics of the XUV beam

The generated harmonic beam is characterized in VC4. The chamber is equipped with a beam routing possibility to characterize the XUV beam with various devices such as pulse energy

Optics EXPRESS

measurement; XUV spectrometer and XUV wavefront sensor (see Fig. 4). Switching between the diagnostics is done by inserting either a toroidal mirror or a flat mirror in the XUV beam or leaving the beam freely propagate. The switching is performed under vacuum using a motorized translation stage.

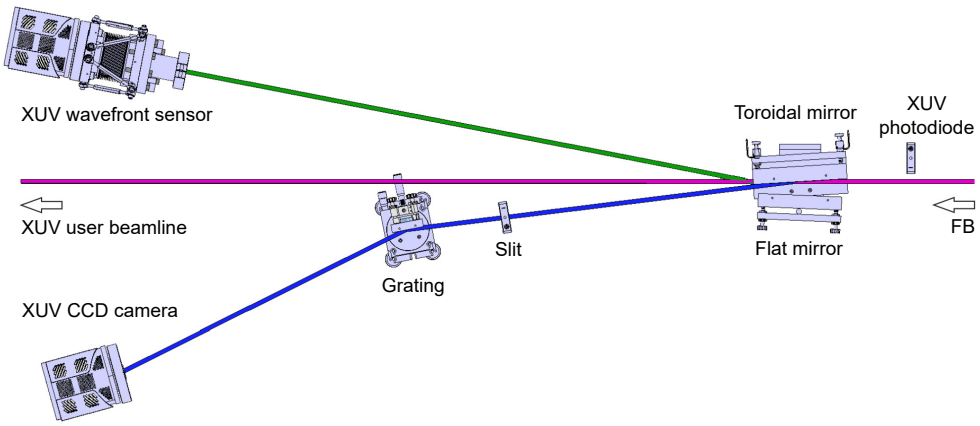


Fig. 4. Schematics of VC4 with XUV spectrometer, wavefront sensor and photodiode.

### 3.1. Measurement of XUV pulse energy

Absolute XUV pulse energy can be obtained from the total charge generated by a calibrated XUV photodiode that can be inserted in the beam after the IR light is already filtered out by the 3 mirrors and metallic filters.

For a reference single-shot measurement of XUV pulse energy a novel method based on the measurement of current pulses from a metallic filter was developed. As the XUV pulse passes through the free-standing filter an electric current is generated due to external photo effect on the filter face and the resultant current pulse can be measured. The total charge carried in the current pulse is proportional to the number of XUV photons passing through the filter. The filter holder is made of steel and is connected to an oscilloscope via a voltage supply and separator circuit. This way, one can set the filter under static voltage to improve the signal.

We present preliminary results of this diagnostic tool measuring the photo-charge from a 420 nm thick aluminum filter generated by a HHG pulses from Ar gas cell. A calibrated XUV diode behind the filter was used to measure the absolute XUV pulse energy of the same shots. A voltage of -80 V was applied on the filter and a current amplifier with an amplification factor of 1000 was used to improve the signal-to-noise ratio. Apart from the fluctuation in the pulse intensity given by laser fluctuations, we varied the gas cell pressure to achieve different XUV pulse energy values. The transmission for wavelengths from 27.8 nm to 42.5 nm (corresponding to $29^{th}$ to $19^{th}$ harmonic orders) ranges from 26% to 19% [19] assuming 4 nm of Al oxide on each side of the filter.

Figure 5 shows the charge measured on the filter as a function of the pulse energy obtained by the XUV photodiode for individual laser shots. The linear dependence of the data shows that it is feasible to measure the pulse energy using this method during user experiments. The offset of the measurement will, however, be a subject of further investigation.

This online measurement method is an alternative to a gas monitor detector where the XUV photons ionize a low-pressure gas in a dedicated chamber and the charged particles are collected [20]. However, our method is much less demanding to install, operate and maintain.

Optics EXPRESS

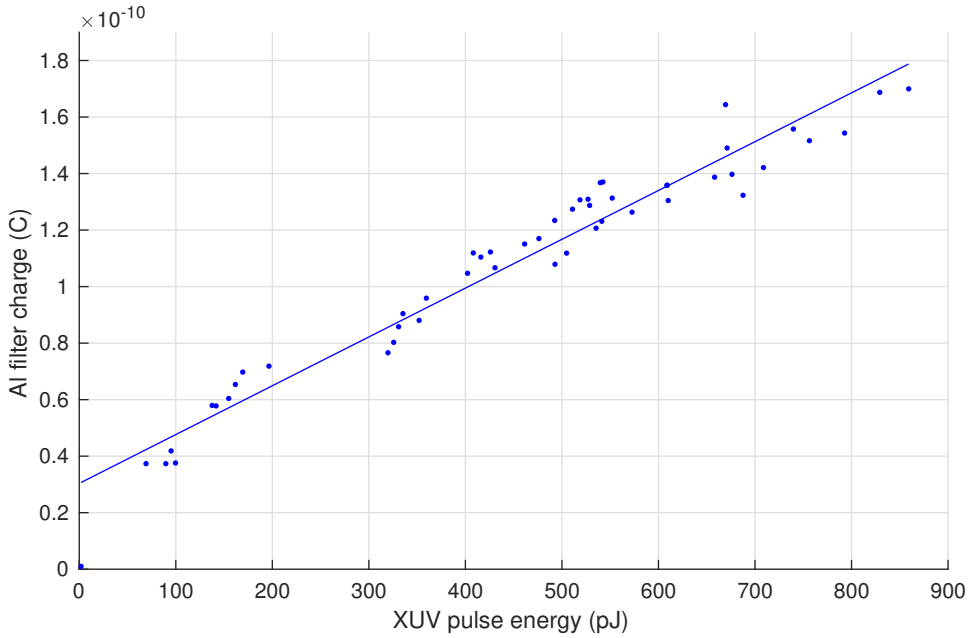


Fig. 5. Dependence of the filter electric charge on the photodiode electric charge for corresponding laser shots. The measurements were performed with -80 V voltage applied on the filter and a $10^3$ amplification with an amplifier bandwidth of 500 kHz. Linear fit ($y = ax + b$) coefficients are $a = 1.73 \times 10^{-13}$ and $b = 3.04 \times 10^{-11}$.

### 3.2. XUV spectrometer

The HHG beam can be also analyzed by unique design high resolution and high sensitivity XUV spectrometer. The total spectral range covered by this instrument is from 5 nm to 120 nm. The spectrometer is composed of a toroidal mirror, a motorized slit of variable width, a reflection grating and a back-illuminated CCD.

The toroidal mirror images the incoming XUV beam onto the slit in the vertical direction. The concave grating with variable line spacing disperses the light angularly and images the slit in the horizontal direction onto the chip of the XUV CCD.

The toroidal mirror with grazing angle of 3.5 degrees and radii of curvature $R_1$ = 10.4 m and $R_2$ = 160 mm is placed 5.2 m from the source at distance 405 mm before the slit giving a demagnification of 12.8 times. The distance from the slit to the grating is 350 mm and the XUV CCD camera is placed 469 mm after the grating. The full spectral range is achieved by two gratings with grazing angle of 4.7 degrees, one with groove density of 1200 lines/mm and the second with 600 lines/mm corresponding to a spectral range 5-60 nm and 20-120 nm, respectively.

The advantage of using the toroidal mirror is a significant increase in the photon flux per pixel, thus increasing the signal-to-noise ratio while not affecting spectral properties of the spectrometer.

Furthermore, imaging with a concave spherical grating suffers from strong astigmatism which is compensated by a properly designed radius $R_2$ of the toroidal mirror. Therefore, the toroidal mirror does not serve only as collecting optics; in the horizontal plane the aberration is also limited by using 2 optical elements. It was shown by ray-tracing simulation that any astigmatism was almost completely compensated and thus the flux on the CCD camera was increased by several orders of magnitude. Figure 6 shows spectral resolution for both gratings estimated from

Optics EXPRESS

these simulations.

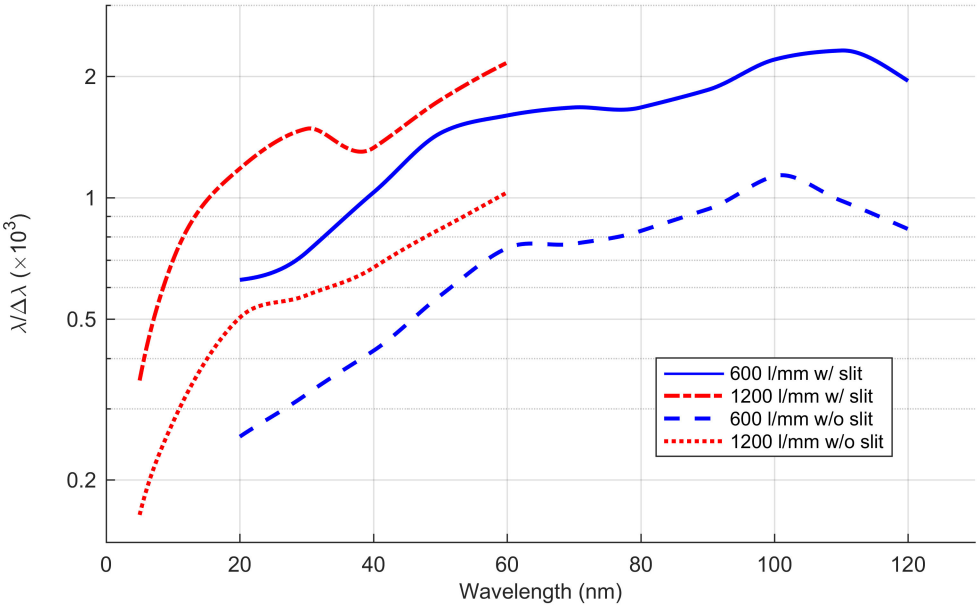


Fig. 6. Spectral resolution of the XUV spectrometer for 600 lines/mm grating without slit (blue dashed), 600 lines/mm grating with slit (blue solid), 1200 lines/mm grating without slit (red dotted) and 1200 lines/mm grating with 20 µm slit (red dash-dotted). The slits are placed in the vertical image plane of the toroidal mirror.

Note that using the toroidal mirror leads to a significant increase of the spectrometer sensitivity in exchange of losing the information on far-field photon energy distribution of the beam. By exchanging the toroidal mirror for a flat mirror one would gain the vertical energy profile in the far-field and lower the overall sensitivity of the spectrometer.

The spectra of pulses generated in neon and argon with Al and Zr filters are shown in Fig. 7.

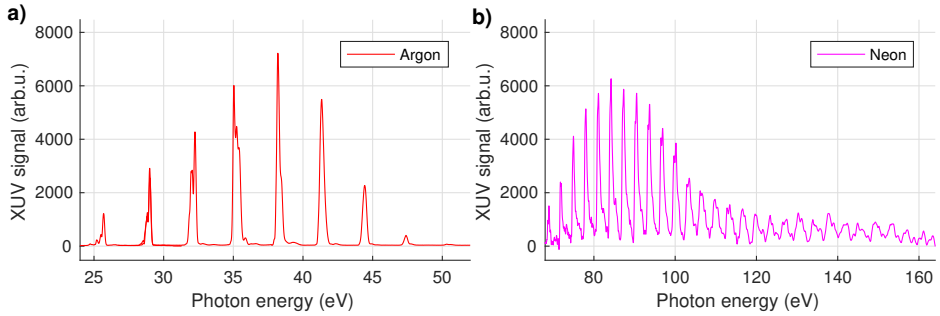


Fig. 7. Measured spectra from the HHG beamline commissioning. The XUV beam was generated a) in argon and b) in neon. Measurements were done with (a) 150 nm thick aluminum filter and b) 300 nm thick zirconium filter.

### 3.3. *Wavefront sensor*

The wavefront of the generated XUV beam is analyzed via a wavefront sensor that is installed under vacuum and mounted at the back of the VC4 (see Fig. 4). The wavefront characterization

Optics EXPRESS

is based on the Hartmann principle where a grid of holes is placed in front of a XUV CCD. The XUV beam transmitted through the grid forms a grid of spots on the CCD and from their position and intensity one can calculate the beam wavefront and intensity profile, respectively.

The device is designed and optimized for coherent XUV beams in the wavelength range from 5 nm to 120 nm (10 - 250 eV). The grid consists of 60 x 60 holes with a pitch of 210 µm at a distance of 43.5 mm in front of the CCD. In the case of a diverging XUV beam the effective number of holes is reduced, however, irradiation of 40 x 40 holes only is sufficient for Zernike polynomials calculation up to the order of 36 [21]. The XUV CCD camera has 1024 x 1024 pixels with a pixel size of 13.5 µm. The distance from the source is 6.2 m resulting in total angular acceptance of the device of 2 x 2 mrad.

The measured absolute wavefront accuracy in the calibrated spectral range is < 1.2 nm RMS resulting in an accuracy better than $\lambda/5$ down to 10 nm wavelength.

The sensor input aperture is 13 x 13 mm and it is capable of measuring the beam wavefront curvatures from infinity (collimated beam) down to 0.45 m. Due to the grid pitch, the spatial sampling of the XUV beam is 210 µm. The wavefront of the XUV beam generated by the ELI Beamlines HHG source was characterized by the setup described above and the results are shown in Fig. 8.

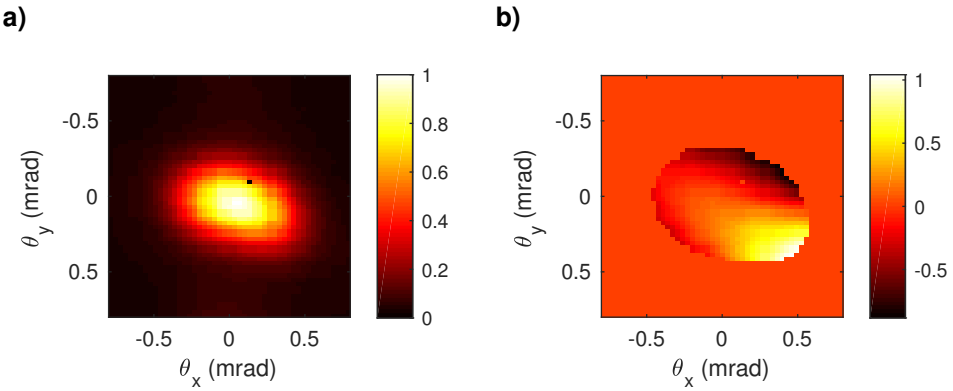


Fig. 8. (a) Spatial profile and (b) wavefront of the XUV beam generated in an argon gas cell. False colors present intensity in arb. units. The wavefront tilt and curvature corresponding to the beam direction and divergence are not included in the wavefront profile.

Figure 8 represents the unoptimized beam generated in argon using $F_{\#} = 250$ resulting in a 0.6 x 0.4 mrad beam (FWHM).

The device can be removed from its original position in the diagnostics chamber (VC4) and used for alignment of a XUV focusing optics at a user experiment.

## 4. HHG monochromator

In the near future, the HHG beamline will be equipped with a grating monochromator. Its design is based on the monochromator setup reported in [22–24].

The monochromator will be placed in between the VC3 and FB. Its principal purpose is to select and transmit chosen wavelength and reduce the bandwidth of the XUV radiation via rotating a reflective diffraction grating and selecting an appropriate slit width. The setup is motorized allowing a convenient change of the transmitted wavelength under vacuum and also the removal of the monochromator optics from the beam axis for free propagation of the broad-spectrum beam to diagnostics chamber or to the straight beamline output arm.

Optics EXPRESS

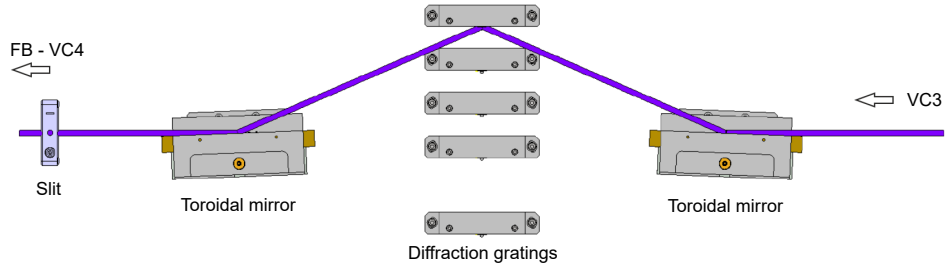


Fig. 9. Schematics of the grating-based monochromator.

### 4.1. Monochromator setup

The schematic of the monochromator is presented in Fig. 9. First, a grazing incidence toroidal mirror collimates the XUV beam that is consequently diffracted by one of four plane diffraction grating with the groove direction in the plane of incidence. After the conical diffraction on the grating only a certain wavelength selected by the tilt of the grating will be focused by the second toroidal mirror on a slit located on the original beam axis. The grazing angle of both toroidal mirrors is 2 deg. The focal lengths of those mirrors are 4.8 m and 2.4 m for collimation and focusing on the slit, respectively. Thus, the slit forms an XUV source with half of its original size and double the divergence. There will be four manually selectable slits of widths 50, 100, 200, and 300 µm to match the required source size and transmitted bandwidth. Two types of refocusing optics are considered following the slit: an ellipsoidal mirror with grazing angle of 5 deg and demagnification factor of 1/4.8; and a toroidal mirror having the same incidence angle in a one-to-one imaging configuration. The focus of this setup will be located in the MAC chamber.

### 4.2. Output pulse parameters

In the single grating configuration described above one cannot avoid a pulse-front tilt, which lengthens the XUV pulse duration. The aim of the optical design is to find the best configuration that gives minimum pulse-front tilt and reasonable spectral resolution while keeping transmission of the setup as high as possible.

The monochromator will work primarily in the spectral range of 10-120 eV. The energy resolution of < 1 eV will be sufficient to separate adjacent harmonics. Gratings listed in Tab. 2 have been found to be suitable for the HHG monochromatization setup.

Table 2. Gratings used for the monochromator and spectral ranges considered for their operation.

| Grating (lines/mm) | Spectral region (eV) |
|---|---|
| G1 (86) | 10-28 |
| G2 (158) | 25-54 |
| G3 (600) | 51-98 |
| G4 (985) | 86-121 |

The energy resolution calculated for a 100 µm slit is shown in Fig. 10(a). The accepted XUV

Optics EXPRESS

beam full divergence is 1 mrad, i.e., the maximum illuminated area on the gratings on direction perpendicular to the grooves is 4.8 mm.

The pulse duration expected with 1 mrad full divergence is shown in Fig. 10(b). Even for a 1 mrad XUV beam, the pulse-front tilt will be below 80 fs, so it may be accepted for a wide range of ultrafast experiments requiring a resolution below 100 fs.

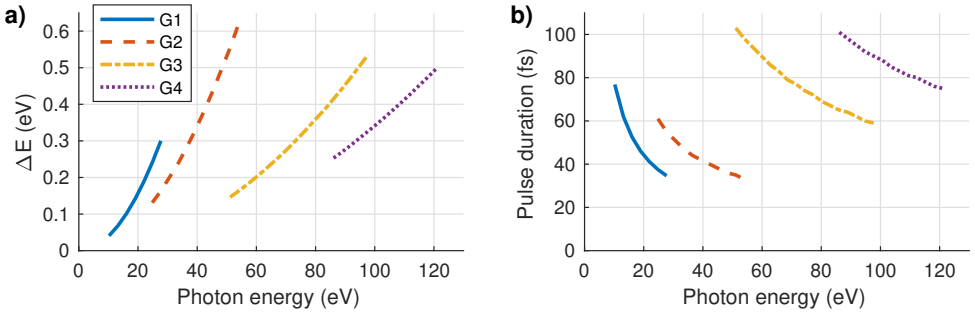


Fig. 10. Energy resolution (a) and pulse duration (b) for 100 µm slit calculated for the gratings listed in Tab. 2 assuming 1 mrad full divergence. G1 solid blue, G2 red dashed, G3 yellow dash-dotted, G4 purple dotted.

## 5. Conclusion and outlook

In conclusion, we have developed a user oriented XUV beamline and implemented it at the ELI Beamlines facility. Currently, it is driven by a Ti:Sapphire based CPA system delivering pulses of 40 fs duration at a repetition rate of 1 kHz with a pulse energy up to 5 mJ. In the near future, the beamline will be driven by 100 mJ, 20 fs pulses generated with a repetition rate of 1 kHz by a Ti:Sapphire based OPA system. The XUV pulses are produced via high harmonic generation in a gas cell in a loose focusing geometry. The focal length and the gas cell length are adaptable to fit the laser driver and target gas type.

We have presented the experimental setup in detail with focus on different focusing and interaction geometries, the IR rejection system and the available characterization techniques including the unique high sensitivity XUV spectrometer and novel online XUV pulse energy monitor. We presented results obtained during instrument commissioning such as the XUV pulse energy, spectrum and wavefront profile.

We also outlined features of the XUV monochromator that the beamline will be upgraded with in the near future. The setup for two XUV beams generated in parallel for advanced pump/probe applications was described as well.

The XUV beamline at ELI Beamlines is a versatile tool that is now available for users that for their applications need an intense, stable and coherent XUV source that can be synchronized with other radiation sources. For user experiments, the XUV beamline is directly connected to a multipurpose station for Atomic, Molecular and Optical science and Coherent Diffractive Imaging (the MAC chamber) and a magneto-optical VUV Ellipsometer that are under implementation. This way, the overall setup of the HHG beamline, MAC chamber and ellipsometer will be able to accommodate cutting edge pump-probe experiments in ultrafast XUV science. Moreover, the experimental hall is designed to be upgraded in a way that THz coherent beams, $K\alpha$ radiation and OPA tunable laser beams will be connected with the HHG source beam to allow users to perform unprecedented pump-probe experiments in an extremely broad wavelength range from THz over mid-IR, visible, XUV to hard X-rays.

Optics EXPRESS

## Funding

Ministerstvo Školství, Mládeže a Tělovýchovy (MŠMT) (LM2015083, LM2015065, LQ1606); European Regional Development Fund (ERDF) ($CZ.02.1.01/0.0/0.0/16_019/0000789$); European Social Fund (ESF) ($CZ.1.07/2.3.00/20.0279$).

## Acknowledgments

We are grateful to A. Wolf and Z. Svoboda for their technical support and M. Morrissey for manuscript revision.

## References

1. A. D. Shiner, B. E. Schmidt, C. Trallero-Herrero, H. J. Wörner, S. Patchkovskii, P. B. Corkum, J.-C. Kieffer, F. Légaré, and D. M. Villeneuve, "Probing collective multi-electron dynamics in xenon with high-harmonic spectroscopy," Nat. Phys. **7**, 464–467 (2011).
2. F. Calegari, D. Ayuso, A. Trabattoni, L. Belshaw, S. D. Camillis, S. Anumula, F. Frassetto, L. Poletto, A. Palacios, P. Decleva, J. B. Greenwood, F. Martin, and M. Nisoli, "Ultrafast electron dynamics in phenylalanine initiated by attosecond pulses," Science **346**, 336–339 (2014).
3. R. L. Sandberg, A. Paul, D. A. Raymondson, S. Hädrich, D. M. Gaudiosi, J. Holtsnider, R. I. Tobey, O. Cohen, M. M. Murnane, H. C. Kapteyn, C. Song, J. Miao, Y. Liu, and F. Salmassi, "Lensless diffractive imaging using tabletop coherent high-harmonic soft-x-ray beams," Phys. Rev. Lett. **99**, 098103 (2007).
4. A. Ravasio, D. Gauthier, F. R. N. C. Maia, M. Billon, J.-P. Caumes, D. Garzella, M. Géléoc, O. Gobert, J.-F. Hergott, A.-M. Pena, H. Perez, B. Carré, E. Bourhis, J. Gierak, A. Madouri, D. Mailly, B. Schiedt, M. Fajardo, J. Gautier, P. Zeitoun, P. H. Bucksbaum, J. Hajdu, and H. Merdji, "Single-shot diffractive imaging with a table-top femtosecond soft x-ray laser-harmonics source," Phys. Rev. Lett. **103**, 028104 (2009).
5. D. Rupp, N. Monserud, B. Langbehn, M. Sauppe, J. Zimmermann, Y. Ovcharenko, T. Möller, F. Frassetto, L. Poletto, A. Trabattoni, F. Calegari, M. Nisoli, K. Sander, C. Peltz, M. J. Vrakking, T. Fennel, and A. Rouzée, "Coherent diffractive imaging of single helium nanodroplets with a high harmonic generation source," Nat. Commun. **8**, 493 (2017).
6. A. Paul, R. A. Bartels, R. Tobey, H. Green, S. Weiman, I. P. Christov, M. M. Murnane, H. C. Kapteyn, and S. Backus, "Quasi-phase-matched generation of coherent extreme-ultraviolet light," Nature **421**, 51–54 (2003).
7. I. J. Kim, G. H. Lee, S. B. Park, Y. S. Lee, T. K. Kim, C. H. Nam, T. Mocek, and K. Jakubczak, "Generation of submicrojoule high harmonics using a long gas jet in a two-color laser field," Appl. Phys. Lett. **92**, 021125 (2008).
8. C. Heyl, H. Coudert-Alteirac, M. Miranda, M. Louisy, K. Kovács, V. Tosa, E. Balogh, K. Varjú, A. L'Huillier, A. Couairon, and C. L. Arnold, "Scale-invariant nonlinear optics in gases," Optica **3**, 75–81 (2016).
9. V. Nefedova, M. Albrecht, M. Kozlová, and J. Nejdl, "Development of a high-flux xuv source based on high-order harmonic generation," J. Electron Spectrosc. Relat. Phenom. **220**, 9–13 (2017).
10. F. Batysta, R. Antipenkov, J. Novák, J. T. Green, J. A. Naylon, J. Horáček, M. Horáček, Z. Hubka, R. Boge, T. Mazanec, B. Himmel, P. Bakule, and B. Rus, "Broadband OPCPA system with 11 mJ output at 1 kHz, compressible to 12 fs," Opt. Express **24**, 17843 (2016).
11. P. B. Corkum, "Plasma perspective on strong field multiphoton ionization," Phys. Rev. Lett. **71**, 1994–1997 (1993).
12. P. Balcou, P. Salières, A. L'Huillier, and M. Lewenstein, "Generalized phase-matching conditions for high harmonics: The role of field-gradient forces," Phys. Rev. A **55**, 3204–3210 (1997).
13. X. He, M. Miranda, J. Schwenke, O. Guilbaud, T. Ruchon, C. Heyl, E. Georgadiou, R. Rakowski, A. Persson, M. B. Gaarde, and A. L'Huillier, "Spatial and spectral properties of the high-order harmonic emission in argon for seeding applications," Phys. Rev. A **79**, 063829 (2009).
14. G. A. Mourou, G. Korn, W. Sandner, and J. L. Collier, *ELI-Extreme Light Infrastructure: Science and Technology with Ultra-Intense Lasers, Whitebook* (Andreas Thoss, 2011).
15. M. Schnürer, Z. Cheng, M. Hentschel, G. Tempea, P. Kálmán, T. Brabec, and F. Krausz, "Absorption-limited generation of coherent ultrashort soft-x-ray pulses," Phys. Rev. Lett. **83**, 722–725 (1999).
16. J.-F. Hergott, M. Kovacev, H. Merdji, C. Hubert, Y. Mairesse, E. Jean, P. Breger, P. Agostini, B. Carré, and P. Salières, "Extreme-ultraviolet high-order harmonic pulses in the microjoule range," Phys. Rev. A **66**, 021801 (2002).
17. L. Strüder, S. Epp, D. Rolles, R. Hartmann, P. Holl, G. Lutz, H. Soltau, R. Eckart, C. Reich, K. Heinzinger, C. Thamm, A. Rudenko, F. Krasniqi, K.-U. Kühnel, C. Bauer, C.-D. Schröter, R. Moshammer, S. Techert, D. Miessner, M. Porro, O. Hälker, N. Meidinger, N. Kimmel, R. Andritschke, F. Schopper, G. Weidenspointner, A. Ziegler, D. Pietschner, S. Herrmann, U. Pietsch, A. Walenta, W. Leitenberger, C. Bostedt, T. Möller, D. Rupp, M. Adolph, H. Graafsma, H. Hirsemann, K. Gärtner, R. Richter, L. Foucar, R. L. Shoeman, I. Schlichting, and J. Ullrich, "Large-format, high-speed, x-ray pnccds combined with electron and ion imaging spectrometers in a multipurpose chamber for experiments at 4th generation light sources," Nucl. Instruments Methods Phys. Res. Sect. A: Accel. Spectrometers, Detect. Assoc. Equip. **614**, 483–496 (2010).

Optics EXPRESS

18. S. Espinoza, G. Neuber, C. D. Brooks, B. Besner, M. Hashemi, M. Ruebhausen, and J. Andreasson, "User oriented end-station on VUV pump-probe magneto-optical ellipsometry at ELI beamlines," Appl. Surf. Sci. **421**, 378–382 (2017).
19. B. L. Henke, E. M. Gullikson, and J. C. Davis, "X-ray interactions: photoabsorption, scattering, transmission and reflection e= 50-30,000 ev, z= 1-92," At. Data Nucl. Data Tables **54**, 181–342 (1993).
20. K. Tiedtke, J. Feldhaus, U. Hahn, U. Jastrow, T. Nunez, T. Tschentscher, S. V. Bobashev, A. A. Sorokin, J. B. Hastings, S. Möller, L. Cibik, A. Gottwald, A. Hoehl, U. Kroth, M. Krumrey, H. Schöppe, G. Ulm, and M. Richter, "Gas detectors for x-ray lasers," J. Appl. Phys. **103**, 094511 (2008).
21. G. Beaugrand and D. Korn, "Calibration report haso euv ha-4627," techreport, Imagine Optic (2014). Property of Imagine Optic, Confidential Information.
22. F. Frassetto, C. Cacho, C. A. Froud, I. C. E. Turcu, P. Villoresi, W. A. Bryan, E. Springate, and L. Poletto, "Single-grating monochromator for extreme-ultraviolet ultrashort pulses," Opt. Express **19**, 19169 (2011).
23. L. Poletto, F. Frassetto, and P. Villoresi, "Ultrafast grating instruments in the extreme ultraviolet," IEEE J. Sel. Top. Quantum Electron. **18**, 467–478 (2012).
24. L. Poletto, P. Miotti, F. Frassetto, C. Spezzani, C. Grazioli, M. Coreno, B. Ressel, D. Gauthier, R. Ivanov, A. Ciavardini, M. de Simone, S. Stagira, and G. D. Ninno, "Double-configuration grating monochromator for extreme-ultraviolet ultrafast pulses," Appl. Opt. **53**, 5879 (2014).